

# Bursting and Quenching in Massive Galaxies without Major Mergers or AGNs

Yuval Birnboim, Avishai Dekel and Eyal Neistein

Racah Institute of Physics, The Hebrew University, Jerusalem 91904 Israel  
*yuval@phys.huji.ac.il; dekel@phys.huji.ac.il; eyal.n@phys.huji.ac.il*

9 March 2018

## ABSTRACT

We simulate the buildup of galaxies by spherical gas accretion through dark-matter haloes, subject to the development of virial shocks. We find that a uniform cosmological accretion rate turns into a rapidly varying disc buildup rate. The generic sequence of events (Shocked-Accretion Massive Burst & Shutdown: SAMBA) consists of four distinct phases: (a) continuous cold accretion while the halo is below a threshold mass  $M_{\text{sh}} \sim 10^{12} M_{\odot}$ , (b) tentative quenching of gas supply for  $\sim 2$  Gyr, starting abruptly once the halo is  $\sim M_{\text{sh}}$  and growing a rapidly expanding shock, (c) a massive burst due to the big crunch of  $\sim 10^{11} M_{\odot}$  gas in  $\sim 0.5$  Gyr, when the accumulated heated gas cools and joins new infalling gas, and (d) a long-term shutdown, enhanced by a temporary shock instability in late SAMBAs, those that quench at  $z \sim 2$ , burst at  $z \sim 1$  and end up quenched in  $10^{12-13} M_{\odot}$  haloes today. The quenching and bursting occur at all redshifts in galaxies of baryonic mass  $\sim 10^{11} M_{\odot}$  and involve a substantial fraction of this mass. They arise from rather smooth accretion, or minor mergers, which, unlike major mergers, may leave the disc intact while being built in a rapid pace. The early bursts match observed maximum starbursting discs at  $z \gtrsim 2$ , predicted to reside in  $\lesssim 10^{13} M_{\odot}$  haloes. The late bursts resemble discy LIRGs at  $z \lesssim 1$ . On the other hand, the tentative quenching gives rise to a substantial population of  $\sim 10^{11} M_{\odot}$  galaxies with a strongly suppressed star-formation rate at  $z \sim 1-3$ . The predicted long-term shutdown leads to red & dead galaxies in groups. A complete shutdown in more massive clusters requires an additional quenching mechanism, as may be provided by clumpy accretion. Alternatively, the SAMBA bursts may trigger the AGN activity that couples to the hot gas above  $M_{\text{sh}}$  and helps the required quenching. The SAMBA phenomenon is yet to be investigated using cosmological simulations.

**Key words:** shock waves — accretion — galaxies: evolution — galaxies: formation — galaxies: haloes — dark matter

## 1 INTRODUCTION

Observations reveal a puzzling phenomenon of “maximum starbursting” in massive galaxies at high redshift in cases where major mergers are ruled out. Examples include LIRGs at  $z \lesssim 1$  (Hammer et al. 2005) and maximum bursters at  $z \gtrsim 2$  (Genzel et al. 2006; Förster Schreiber et al. 2006). In these cases, galaxies of stellar masses  $\sim 10^{11} M_{\odot}$  seem to be forming a large fraction of their stars at a star-formation rate  $\text{SFR} \sim 100-200 M_{\odot} \text{yr}^{-1}$  within  $\sim 0.5$  Gyr. This is much shorter than the age of the universe then, indicating coherent star formation from  $\sim 10^{11} M_{\odot}$  of gas in the latest stages of its collapse/assembly rather than in its earlier smaller progenitors. Furthermore, the burst duration is significantly shorter than the time implied by the typical cos-

mological accretion rate onto haloes of  $\sim 10^{12} M_{\odot}$  at the relevant epochs, and is as short as the time for streaming at the virial velocity from the virial radius to the center. Gaseous major mergers, which could have provided such rapid bursts, are unlikely in many of these cases, where the galaxies are detected to be relatively smooth, rotating, thick discs that could not have survived a major merger and show no trace of such an event. At the low end of the SFR distribution, most galaxies of stellar mass  $M_{\text{d}} \geq 10^{11} M_{\odot}$  tend to be quenched red & dead galaxies, and a substantial fraction of such galaxies show strongly suppressed star-formation rates (SFR) already at high redshifts,  $0.5 < z < 2.7$  (Kriek et al. 2006; Noeske et al. 2007). We seek an explanation for these phenomena at the two extreme regimes of SFR.

We report here on new insight gained from spherical modeling of gas accretion onto massive galaxies, which could be the basis for understanding the above phenomena and other central issues in galaxy formation.

Following the classic work on the interplay between cooling and dynamical times in galaxy formation (Rees & Ostriker 1977; Silk 1977; Binney 1977; White & Rees 1978; Blumenthal et al. 1984), we used analytic calculations and hydrodynamical simulations to study the evolution of a virial shock in a spherical configuration (Birnboim & Dekel 2003; Dekel & Birnboim 2006). We predicted the existence of a threshold halo mass for the presence of a virial shock, at  $M_{\text{sh}} \sim 10^{12} M_{\odot}$ , roughly independent of redshift. Less massive haloes do not permit a stable shock, as rapid radiative cooling prevents the hypothetical post-shock gas pressure from supporting the shock against global gravitational collapse into the halo center. The gas accreting through the virial radius of such haloes flows cold ( $\sim 10^4 \text{ K}$ ) into the inner halo, where it may eventually shock, feed a disc and efficiently form stars. Once the halo grows above  $M_{\text{sh}}$ , a stable shock emerges from the inner halo and rapidly propagates toward the virial radius, halting the infalling gas and creating a hot medium in quasi-static equilibrium at the halo virial temperature. We found that the transition to stability occurs when the standard radiative cooling time at the assumed metallicity equals the time for compression behind the shock,  $t_{\text{comp}} = (21/5)\rho/\dot{\rho} \simeq (4/3)R/V$ , where  $\rho$  is the gas density behind the shock,  $R$  is the shock radius and  $V$  is the infall velocity into the shock.

Based on these findings, it has been proposed that the presence of hot, dilute gas allows the suppression of gas supply to the disc, possibly assisting AGN feedback, and thus leads to quenching of star formation (Binney 2004; Dekel & Birnboim 2006). This mass threshold has proven to be the key for understanding the robust division of galaxies into blue, star-forming discs versus red & dead spheroids and their basic properties (Dekel & Birnboim 2006; Cattaneo et al. 2006; Croton et al. 2006).

The success of the spherical model in predicting the threshold mass as seen in cosmological hydrodynamical simulations (Kereš et al. 2005; Dekel & Birnboim 2006) is demonstrated in Fig. 1, which summarizes the results of Birnboim et al. (2007). It shows as a function of halo mass the fraction of cold gas within the virial radius and outside the disc in dark-matter haloes from cosmological simulations by A. Kravtsov (described in Kravtsov 2003; Kravtsov & Gnedin 2005, where they were used for other purposes). At all redshifts, there is a transition from cold-dominated haloes to hot-dominated haloes near  $5 \times 10^{11} M_{\odot}$ . This is compatible with the threshold mass predicted by Dekel & Birnboim (2006) for realistic halo metallicities that gradually grow to  $Z \simeq 0.1$  solar today.

This success of the spherical model motivates our present, more detailed and daring investigation of the spherical configuration. We study how the development of the virial shock converts an otherwise uniform accretion through the virial radius into a rapidly varying accretion rate onto the inner disc. The resultant

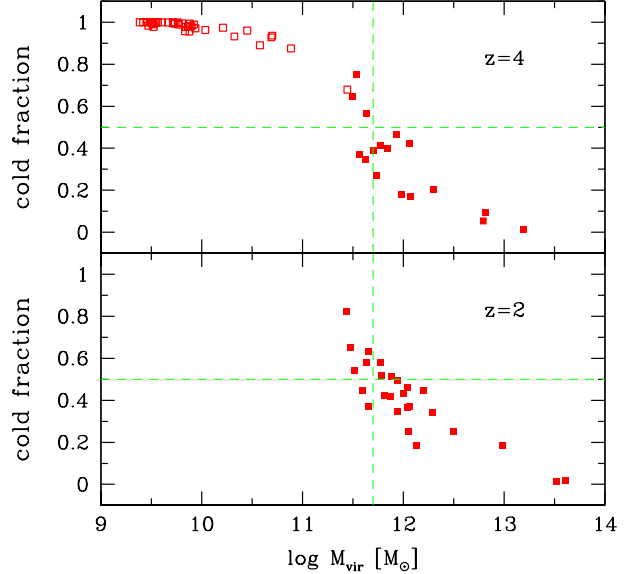


**Figure 1.** The threshold halo mass for virial shock heating in cosmological hydro simulations, at different redshifts, based on (Birnboim et al. 2007). Each point represents the fraction of cold gas within  $0.1R-R$  in a different halo, for haloes above a minimum mass due to numerical resolution. The smaller haloes (open symbols) are drawn from a high-resolution simulation in a box of comoving size  $6 h^{-1}\text{Mpc}$ , which was terminated at  $z = 4$  and therefore do not show counterparts at later redshifts. The more massive haloes (solid symbols) come from a simulation of a lower resolution in a box of  $80 h^{-1}\text{Mpc}$ . Cold gas is defined here by  $T < 10^4 + 0.4(T_{\text{vir}} - 10^4)$ , e.g.,  $T < 2.5 \times 10^5 \text{ K}$  for  $M \simeq 10^{12} M_{\odot}$ , where  $T_{\text{vir}} \simeq 6 \times 10^6 \text{ K}$ . The transition from cold dominance to hot dominance occurs near  $5 \times 10^{11} M_{\odot}$  at all redshifts (vertical line), as predicted by the spherical model for similar metallicities (Dekel & Birnboim 2006).

disc buildup, and the induced SFR, evolve through a generic sequence of events involving two quenching episodes and a massive burst, which always starts at the crossing of the halo threshold mass, namely in galaxies of  $M_d \sim 10^{11} M_{\odot}$  at any redshift. We term this phenomenon SAMBA, for Shocked-Accretion Massive Burst and Shutdown.

In §2 we describe the simulation method. In §3 we present the four phases of the SAMBA phenomenon. In §4 we dare a tentative comparison to observations. In §5 we describe SAMBA recipes for semi-analytic modeling. In §6 we discuss our results. In §A, related to §2, we provide an EPS estimate of the average virial accretion rate onto dark haloes. In §B, related to §5, we specify the SAMBA recipes for SAMs.

## 2 METHOD OF SIMULATIONS

### 2.1 The Spherical hydrodynamical code

Our accurate 1-D Lagrangian hydrodynamical code (based on the code described in Birnboim & Dekel 2003) simulates a spherical gravitating system consisting of dark matter and a fraction  $f_b$  of gas with a constant metallicity  $Z$ . The initial smooth density-

perturbation profile is constructed such that it produces the desired average accretion rate at the virial radius, §2.2. The dissipationless dark-matter shells detach from the cosmological expansion, collapse and oscillate into virial equilibrium such that they deepen the potential well attracting the dissipating gas shells. The gas is cooling radiatively based on the atomic cooling function computed by Sutherland & Dopita (1993), and contracts dissipatively into the inner halo. The collapse of each gas shell is stopped at  $\sim 5\%$  of the virial radius by an artificial centrifugal force which mimics the formation of a central disc.

The main improvements to the original code described in Birnboim & Dekel (2003) are as follows. The numerical scheme for time evolution now computes the pressure and energy of the gas shells within the forth-order Runge Kutta solution rather than externally. A force corresponding to the cosmological constant  $\Lambda$  has been added to the force equations, making the calculation fully consistent with the  $\Lambda$ CDM cosmology, though with only minor effects on the evolution inside the haloes. The simulations described here consist of 1,000 gas shells and 5,000 dark-matter shells, corresponding to a spatial resolution of  $\sim 50$  pc in the inner halo growing to  $\sim 1$  kpc near the virial radius. The energy conservation level, set by the timesteps and spatial resolution, is better than 2% over today's Hubble's time. Convergence tests of some of the runs with twice the spatial resolution yielded very similar results. The baryonic fraction  $f_b$  is assumed to be 10% throughout the simulations presented here, crudely taking into account certain gas mass loss due to feedback effects. Simulations with  $f_b = 0.05\%$  and 0.15% yield consistent results.

## 2.2 Cosmological accretion rate

The average fractional accretion rate onto haloes of mass  $M$  at time  $t$  is estimated in §A using the EPS formalism, following Neistein et al. (2006). Eq. (A5) reads

$$\frac{\dot{M}}{M}(M, t) = s(M) \frac{\delta_c \dot{D}}{D D}, \quad (1)$$

$$s(M) \equiv \left[ \frac{2/\pi}{\sigma^2(M/q) - \sigma^2(M)} \right]^{1/2}. \quad (2)$$

Here  $\sigma(M)$  is the rms linear density fluctuation on the scale corresponding to mass  $M$ , linearly extrapolated to  $z = 0$  using the linear growth function  $D(t)$  normalized to unity at  $t_0$ . The constants are  $\delta_c \simeq 1.68$  from the spherical collapse model, and  $q \simeq 2.2$  reflecting an intrinsic uncertainty in the EPS formalism. The accretion time  $(\dot{M}/M)^{-1}$  is shown later on in Fig. 8 for haloes of  $10^{12} M_\odot$  in the  $\Lambda$ CDM cosmology. A practical approximation for haloes of  $\sim 10^{12} M_\odot$  in  $\Lambda$ CDM is

$$\frac{\dot{M}}{M}(M, t) = 0.04 \text{ Gyr} \left( \frac{M}{10^{12} M_\odot} \right)^{0.15} (1+z)^{2.25}. \quad (3)$$

The mass growth history of the main progenitor of a halo that ends up with mass  $M_0$  at time  $t_0$  is given by eq. (A9):

$$M(t|M_0) = F^{-1}[\delta_c(D^{-1} - 1) + F(M_0)], \quad (4)$$

where  $F^{-1}$  is the inverse function of

$$F(M) = \int_M^\infty \frac{dm}{m s(m)}. \quad (5)$$

We specify in §A the details of this calculation in  $\Lambda$ CDM.

The initial conditions of the simulation specify the mean density profile of the spherical perturbation  $\bar{\delta}_i(M)$ , referring to spheres of mass  $M$  at an initial time  $t_i$  in the linear regime. In order to end up with a halo mass  $M_0$  at  $t_0$ , and have the proper average virial accretion rate throughout the halo history, we invert  $M(t)$  from eq. (4) to a collapse time for mass  $M$ ,  $t_c(M)$ , and then derive the initial profile from

$$\bar{\delta}_i(M) = \delta_c \frac{D(t_i)}{D[t_c(M)]}. \quad (6)$$

## 3 FOUR PHASES OF ACCRETION

### 3.1 Generic SAMBA

Figures 2, 3 and 4 present the SAMBA phenomenon in three simulations, spanning a range of final halo masses. They display the radii of gas shells as they fall through the virial radius and eventually accrete onto the inner disc. One may tentatively and very crudely identify the disc buildup rate with maximum SFR. We see that every SAMBA consists of four distinct phases, as follows:

1. **Cold accretion.** As long as the halo mass is below  $M_{sh}$  there is no stable shock in the halo. The gas flows cold and unperturbed toward the disc following the cosmological accretion rate at the virial radius, which is constructed here to be rather uniform. The resultant disc accretion rate is growing gradually with time, while the specific  $\dot{M}_d/M_d$  is declining. For example, in the late SAMBA shown in Fig. 2, the cold accretion phase lasts till  $t \simeq 4.6$  Gyr, with the temperature map showing no heating and the disc accretion rate rather uniform.

2. **Tentative quenching.** A shock forms near the disc upon crossing  $M_{sh}$ , and it propagates outward very rapidly. The gas that falls through the shock during its rapid expansion is heated and halted to a stop (sometimes even pulled back) before it cools and rains down. A first phase of suppressed disc accretion lasts for 1–2 Gyr, e.g. between  $t \simeq 2.7$  and 4.3 Gyr in Fig. 3.

3. **Massive burst.** The gas that was slowed down in the previous quenching phase now joins new accreting gas in a big crunch onto the disc. The accumulation of shells in a massive crunch results from the longer delay suffered by gas that falls in through the shock earlier, when the shock expands faster. The crunch is enhanced further when the shock develops a temporary instability causing it to contract back to sub-virial radii. Thus,  $\sim 10^{11} M_\odot$  of gas enter the disc during  $\sim 0.5$ –1 Gyr, producing a burst of  $\dot{M}_d \sim 100$ – $200 M_\odot \text{ yr}^{-1}$ , or  $\dot{M}_d/M_d \sim 1$ – $2$ , typically twice the specific virial accretion rate.

4. **Post-burst slowdown or shutdown.** The halo

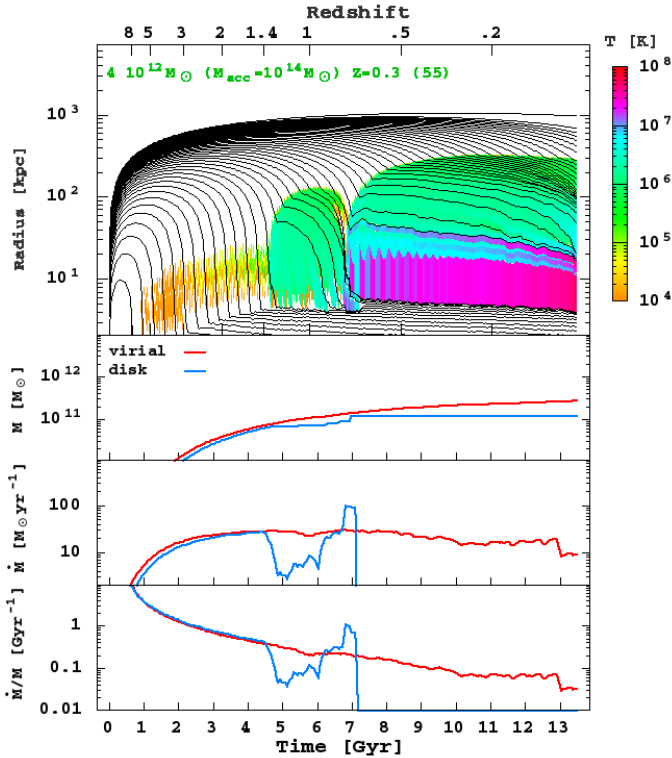


**Figure 2.** Spherical accretion onto the outer dark halo and the inner ‘disc’. **Top:** Infalling gas shells, with the temperature highlighting the evolution of the virial shock. **Bottom:** baryonic mass growth, accretion rate and specific accretion rate (smoothed over a virial crossing time), at the virial radius (red curve) and at the ‘disc’ (blue curve). A **late** SAMBA: today’s halo mass  $M_0 = 4 \times 10^{12} M_\odot$ , metallicity  $Z = 0.3$  and a reduced accretion rate, leading to a tentative quenching onset at  $z_1 \simeq 1.1$ , a burst at  $z_b \simeq 0.7$  with efficiency  $B \simeq 5$ , followed by very effective long-term quenching.

mass is safely above the threshold, with the cooling rate significantly slower than the compression rate, allowing the shock to join the gradual expansion of the virial radius. Bursts that occur prior to  $z \sim 1.4$  are followed by a long period of gradually declining specific accretion rate, which is comparable to the specific virial accretion rate. Bursts that occur after  $z \sim 1.4$  are followed by an effective long-term shutdown from  $z \sim 0.7$  and on, lasting for several Gyr. The infall is halted effectively while crossing the shock during its second expansion phase.

The timing of the SAMBA events scales with the onset time,  $t_1$ . A relevant characteristic time scale at that epoch is the virial crossing time, the time it takes to stream at the virial velocity from the halo virial radius to the center. Based on the spherical collapse model, it is independent of mass and given by<sup>1</sup>

$$t_{\text{vir}} \equiv \frac{R_v}{V_v} \simeq 2.49 \text{ Gyr} (1+z)^{-3/2}. \quad (7)$$

<sup>1</sup> For a proper virial radius,  $(1+z)^{-1}$  should be replaced by  $(\Delta_{200} \Omega_{m,0.3} h_{0.7}^2)^{-1/3} (1+z)^{-1}$ . In a flat universe  $\Delta(a) \simeq [18\pi^2 - 82\Omega_\Lambda(a) - 39\Omega_\Lambda(a)^2]/\Omega_m(a)$ , with  $a = (1+z)^{-1}$ ,  $\Omega_m(a)$  given in §A and  $\Omega_\Lambda = 1 - \Omega_m$ .

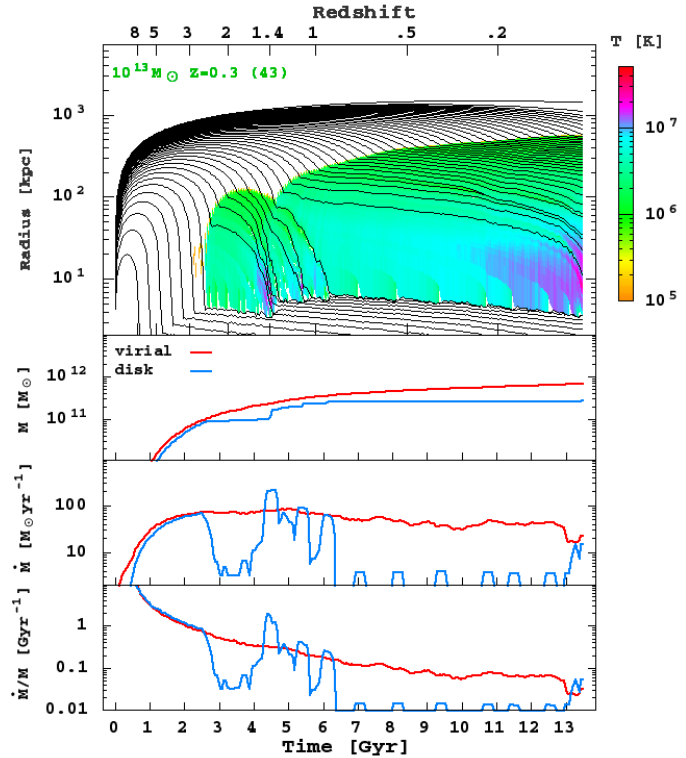


**Figure 3.** Same as Fig. 2 for an **intermediate** SAMBA:  $M_0 = 10^{13} M_\odot$ ,  $Z = 0.3$ , typical accretion rate,  $z_1 \simeq 2.5$ ,  $z_b \simeq 1.4$  with  $B \simeq 6$ , followed by effective long-term quenching.

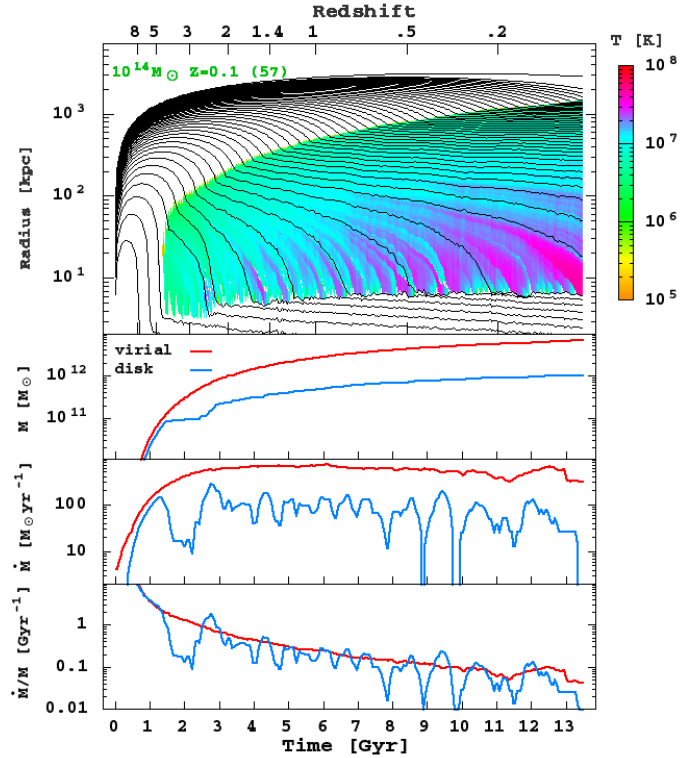


**Figure 4.** Same as Fig. 2 for an **early** SAMBA:  $M_0 = 10^{14} M_\odot$ ,  $Z = 0.1$ , typical accretion rate,  $z_1 \simeq 4.8$ ,  $z_b \simeq 2.5$  with  $B \simeq 2.3$ , followed by ineffective quenching.

In the EdS phase of cosmological evolution (valid to a good approximation prior to  $z \sim 1$ ),  $t_{\text{vir}} \simeq 0.18t_{\text{Hubble}}$ .

We define the efficiency of disc accretion by the ratio of specific accretion rate into the disc and into the virial radius,

$$B \equiv \frac{\dot{M}_d/M_d}{M/M} . \quad (8)$$

A smoothed version of this quantity over a virial crossing time,  $B_v$ , which can be read as the ratio of the two curves shown at the bottom panels of Figs. 2-4, serves us for an automatic identification of the four phases. This quantity is about unity during the cold-flow phase. We mark by  $t_1$  the time when  $B_v$  starts its first drop below unity due to the shock onset. Then  $t_2$  and  $t_3$  mark the subsequent crossings of unity upward and downward, which we define as the beginning and the end of the burst. Finally, we identify the following upward crossing of unity, at  $t_4$ , as the end of the long-term quenching phase, when such a phase exists.

There are several robust SAMBA characteristics that only weakly depend on the redshift of the event. The onset of the SAMBA is always at the crossing of the threshold halo mass,  $M_{\text{sh}} \sim 10^{12} M_{\odot}$ , thus involving a stellar mass  $M_d \sim 10^{11} M_{\odot}$ . The burst peaks about half a Hubble time (1.5 – 2.5 Gyr) later, and involves  $\lesssim 10^{11} M_{\odot}$  of rapidly accreting gas in about a virial crossing time  $t_{\text{vir}}$  ( $\sim 0.5$ –1 Gyr). The average burst efficiency is  $B_v \simeq 2$ , with a peak value of  $B \sim 6$ .

### 3.2 Systematic redshift dependence

By simulating the accretion histories of haloes that end up with different masses  $M_0$  today, we obtain a sequence of SAMBAs with a range of starting times,  $t_1$ , given that the SAMBA onset is determined by the crossing of a fixed halo mass threshold. Our fiducial case assumes the average virial accretion history onto haloes  $M_0$  and a constant metallicity  $Z = 0.3$  solar; we obtain somewhat earlier (later) onset times by lowering (raising)  $Z$  or by raising (lowering) the virial accretion rate at the relevant epoch. It turns out that our current fiducial choice of  $Z = 0.3$  at all times does not follow the gradual cosmological growth of metallicity with time as estimated in Dekel & Birnboim (2006). This results in an artificial overestimate of  $M_{\text{sh}}$  at high  $z$ , by a factor  $\sim 2$ , which we should scale out when considering the cosmological redshift dependence of the SAMBAs.

The characteristic times of 15 simulated SAMBAs are shown in Fig. 5. These times naturally scale with the Hubble time. The burst duration is always  $\Delta t_b \simeq 0.18t_2 \simeq t_{\text{vir}}$ . The duration of the tentative quenching is  $\Delta t_q \simeq 0.8t_1$  for  $z_1 > 2.5$  and  $\Delta t_q \simeq 0.36t_1$  for  $z_1 \leq 2.5$ . The systematic variations with the onset time are primarily driven by the gradual decline with time of the specific virial accretion rate, which induces a drastic change between SAMBAs that start prior to  $z \simeq 2.5$  and those that start later. This is a distinction between the central galaxies of today's clusters of  $> 10^{13} M_{\odot}$  haloes and the more isolated galaxies in today's groups of  $\leq 10^{13} M_{\odot}$  haloes. The former burst

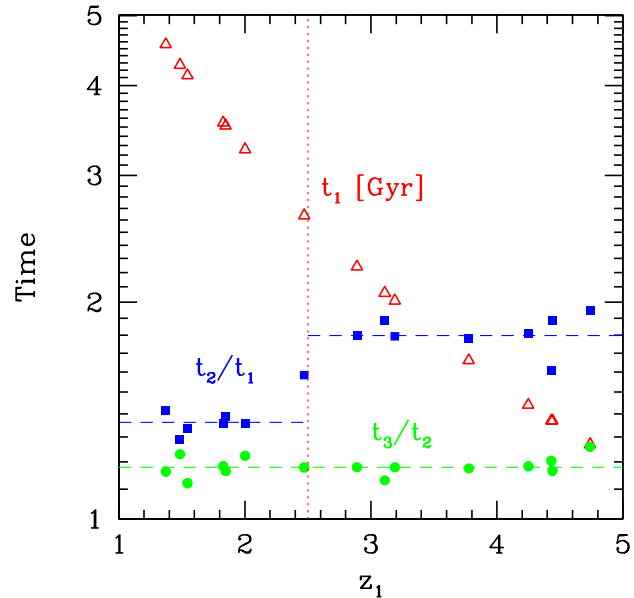


**Figure 5.** Characteristic times of simulated SAMBAs as a function of the onset redshift  $z_1$ , when  $M = M_{\text{sh}}$ . The Hubble time at the onset of tentative quenching is  $t_1$  (open red triangles). The ratio  $t_2/t_1$  (filled blue squares) refers to the duration of the tentative quenching. The ratio  $t_3/t_2$  (filled green circles) refers to the duration of the burst, with  $t_3$  the beginning of long-term quenching in late SAMBAs. The vertical line marks the transition from early to late SAMBAs. The horizontal lines mark the fits used for the SAM recipe in §5.

before  $z \sim 1.4$ , when  $\dot{M}/M > 1 \text{ Gyr}^{-1}$ , while the latter burst later, when  $\dot{M}/M < 1 \text{ Gyr}^{-1}$ . In the late SAMBAs, the rapidly expanding shock overshoots to outside the virial radius, where the low accretion rate fails to provide enough post-shock compression for support against contraction. The resultant temporary instability makes the shock drop to sub-virial radii before the pressure behind it can push it back to the virial radius. Apparently, this instability appears once the specific virial accretion rate drops below  $1 \text{ Gyr}^{-1}$ .

The effect of the virial accretion rate on the tentative shock instability is clearly demonstrated in Figs. 2–4. The strength of the instability as measured by the tentative shrinkage of the shock to sub-virial radii, as seen in the top panels, is correlated with the specific virial accretion rate at shock onset, which could be read from the red curve at the bottom panels or from the inverse of the accretion time shown in Fig. 8. This trend is valid for the whole suite of simulated SAMBAs.

Other quantities characterizing the tentative quenching and the subsequent burst are summarized in Figs. 6 and 7. Most of the burst characteristics vary gradually with the burst time  $t_b \equiv 0.5(t_2 + t_3)$ , and show a bimodality to early and late bursts separated at  $z \simeq 1.4$ , associated with the shock instability. While in the late bursts the disc mass is  $M_d \sim 10^{11} M_{\odot}$ , it is typically twice as large in the early burst, where the specific accretion rate is higher and the preceding quenching is less efficient. The fraction of disc mass involved in the burst between  $t_2$  and  $t_3$ ,  $\Delta M_d/M_d$ , varies from  $\sim 0.7$  in

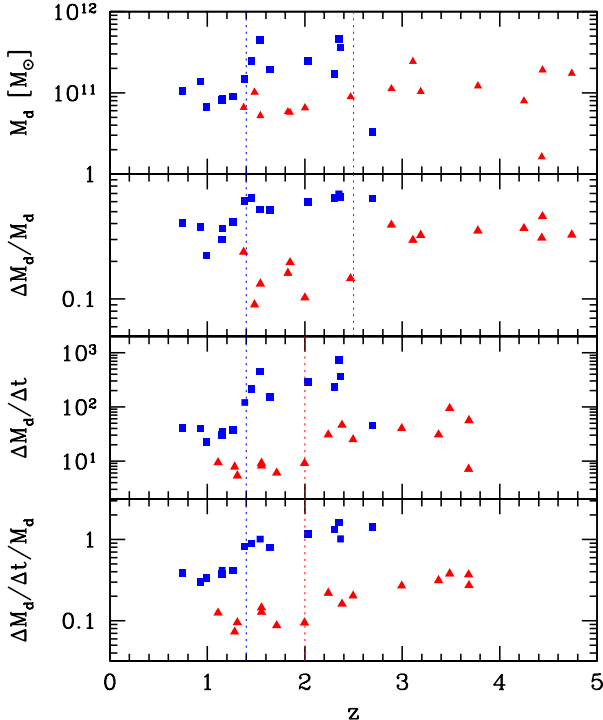


**Figure 6.** SAMBA properties as a function of redshift: disc accretion properties. Red triangles refer to the tentative quenching, at  $z_1$  (top panels) or  $z_q \equiv 0.5(z_1 + z_2)$  (bottom panels). Blue squares refer to the burst at  $z_b \equiv 0.5(z_2 + z_3)$ . Vertical lines separate early from late SAMBAs. From top to bottom: disc mass, fractional disc growth, accretion rate, and specific accretion rate.

the early bursts to  $\sim 0.3$ - $0.4$  in the late ones. The mean specific accretion rate,  $(\Delta M_d/\Delta t)/M_d$ , varies from  $\sim 1$ - $1.5$  to  $\sim 0.4$  Gyr $^{-1}$ . This corresponds to a drop of the average accretion rate across the burst from  $\dot{M}_d \sim 100$ - $400 M_\odot \text{yr}^{-1}$  in the early bursts to  $\sim 30$ - $40 M_\odot \text{yr}^{-1}$  in the late bursts. The average burst efficiency over the burst is always  $B_b = (\Delta M_d/M_d)/(\Delta M/M) \simeq 2$ , while the peak efficiency changes from  $\sim 2$  in the early bursts to 3-6 in the late bursts.

The ratio of virial to disc mass at the end of the burst is bi-modal: It is high for the early bursts,  $M/M_d \sim 25$ - $50$ , and low for the late bursts,  $M/M_d \sim 10$ - $15$ . The high values in the early bursts is because the high virial accretion rate there leads to a rapid halo growth during the quenching phase combined with the failure of the subsequent burst to consume most of the accumulated hot gas. In the late SAMBAs, on the other hand, the halo growth is slow and the burst consumes all the available gas, leading to a low  $M/M_d$ . The early bursts are thus predicted to reside in *very massive haloes*, of  $M \lesssim 10^{13} M_\odot$ , while the late bursts are to be found in  $\sim 10^{12} M_\odot$  haloes.

The characteristics of the *tentative quenching* phase also vary gradually with  $t_1$ . At the onset of all SAMBAs,  $M \sim 10^{12} M_\odot$  and  $M_d \sim 10^{11} M_\odot$ , and we should scale out the apparent slight decline with time of these masses, which is largely an artifact of the assumed constancy of metallicity with time. The typical quenching efficiency is  $B \sim 0.3$  for the early SAMBAs and  $B \sim 0.4$

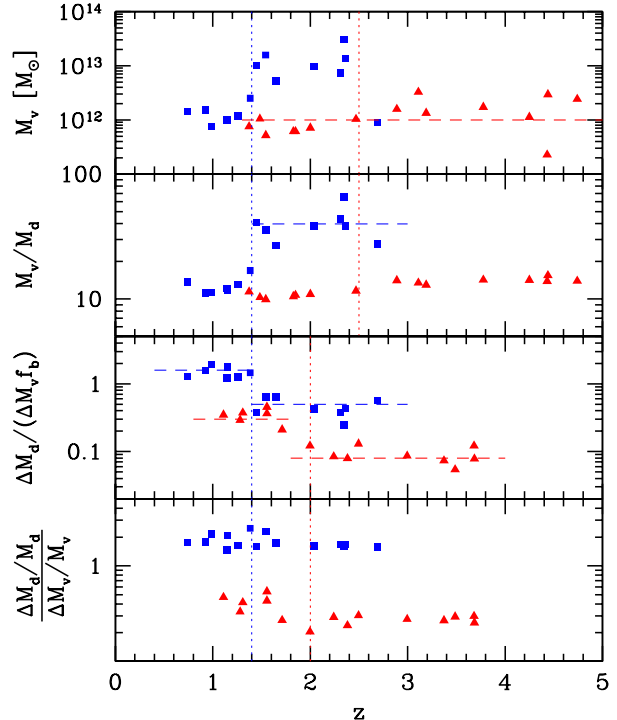


**Figure 7.** SAMBA properties as in Fig. 6: disc versus virial accretion. From top to bottom: virial mass, virial-to-disc mass ratio, disc-to-virial accretion ratio and efficiency  $B$  of specific-accretion ratio. Horizontal lines mark the fits used for SAM recipes in §5.

for the late ones. The ratio of disc to virial gas accretion rate,  $\Delta M_d/(\Delta M f_b)$  varies from  $\lesssim 0.1$  to  $\sim 0.3$  in the early and late SAMBAs respectively, separated at onset redshift  $z \simeq 2.5$ . The tentative quenching can make the galaxy appear red for  $\sim 1$  Gyr before bursting.

The most pronounced effect of the shock instability occurring in the late SAMBAs is a drastic *shutdown* of disc accretion for several Gyr after the burst, starting at  $z \simeq 1.2$  or later. The infalling gas is halted and pushed back after crossing the shock during its second rapid expansion phase, and the fact that the halo is already well above  $M_{\text{sh}}$  makes the cooling and infall time long. These galaxies, in haloes  $\lesssim 10^{13} M_\odot$  today, will appear red & dead at  $z \lesssim 1$ , without the help of any additional feedback effect. On the other hand, the post-burst phase of the early SAMBAs is characterized by a disc specific accretion rate that fluctuates about the virial rate,  $B \sim 1$ . For these central cluster galaxies today to become red & dead one should appeal to another quenching mechanism that could provide long-term maintenance.

## 4 COMPARISON WITH OBSERVATIONS

### 4.1 Maximum Bursting Disks

Two relevant examples of observed “maximum bursters” stand out. First, rest-frame UV/optically-selected star forming galaxies at  $z \gtrsim 2$  (termed BX and BzK). A high-resolution adaptive-optics IR study of BzK-15504 at  $z \simeq 2.4$  (Genzel et al. 2006) reveals  $M_d \simeq 8 \times 10^{10} M_\odot$  plus  $M_{\text{gas}} \simeq 4 \times 10^{10} M_\odot$  forming stars

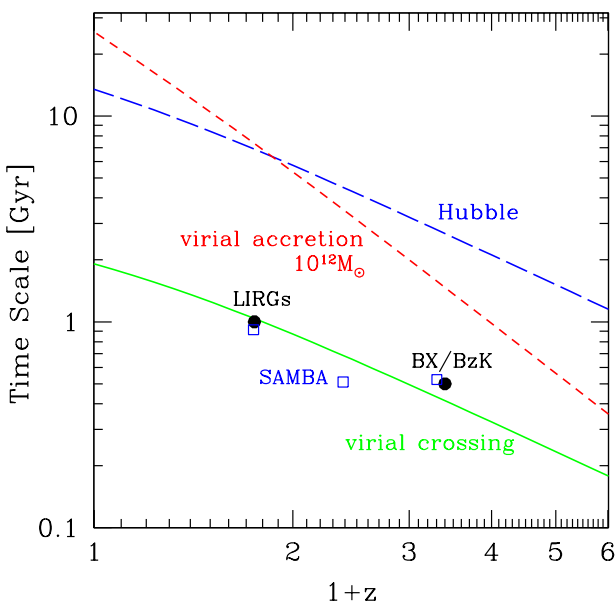


**Figure 8.** Characteristic time scales as a function of redshift. The curves refer to (a) the Hubble time (blue, long dash), (b) the average cosmological accretion time onto  $M = 10^{12} M_{\odot}$  haloes (red, short dash), and (c) rapid streaming from the virial radius to the center,  $R/V$  (green, solid). The estimated duration of the observed maximum starbursts are represented by black circles. The predicted duration of three SAMBA bursts are marked by blue open squares.

at  $\sim 100\text{--}200 M_{\odot}\text{yr}^{-1}$ . The stellar population has a typical age of only  $\sim 0.5$  Gyr, less than 20% of the Hubble time at that epoch. The morphology and kinematics fit an exponential disc of scale radius  $\simeq 4.5$  kpc rotating at  $V_{\text{rot}} \simeq 230 \text{ km s}^{-1}$ , and a recent major merger is ruled out. The velocity dispersion of  $\sigma \simeq 60\text{--}110 \text{ km s}^{-1}$  indicates a rapid accretion onto the disc, again of  $\sim 0.5$  Gyr. Several galaxies with similar properties were detected in a lower resolution study (Förster Schreiber et al. 2006).

Other examples are found among the LIRGs at  $z \sim 0.6\text{--}0.9$ . Hammer et al. (2005) have detected at least six galaxies of  $M_d \sim 10^{11} M_{\odot}$  forming stars at  $\simeq 120\text{--}200 M_{\odot}\text{yr}^{-1}$  while their morphologies and kinematics resemble spiral galaxies with no trace of major mergers. More than half of their IR-luminous galaxies are spirals. The compilation of SFR at  $z \sim 1$  by Noeske et al. (2007) reveals some massive galaxies that form stars at  $\sim 200 M_{\odot}\text{yr}^{-1}$ , while only  $\sim 7\%$  of the galaxies show evidence for ongoing major mergers (Lotz et al. 2006), and this fraction is not higher for the galaxies with the highest SFR (private communication).

In summary, the observed maximum bursters show the following robust features: (a) the baryonic mass is on the order of  $M_d \sim 10^{11} M_{\odot}$ , (b) a substantial fraction of the baryonic mass is bursting, (c) the burst is short compared to the Hubble time and the cosmological mean accretion time, and is comparable to the virial crossing time, (d) the star formation occurs in an extended configuration of a few kpc, and (e) in many cases there are morphological and kinematical indications for a thick rotating disc with no trace of major mergers.

A distinct feature of the maximum bursters is that

most of the stars of the  $M_d \sim 10^{11} M_{\odot}$  galaxies have formed over a short period of time just prior to the observed epoch,  $\sim 0.5$  Gyr at  $z \gtrsim 2$  and  $\sim 1$  Gyr at  $z \lesssim 1$ . This is compared in Fig. 8 to several relevant characteristic timescales. The burst duration is shorter than the age of the universe at that time by a factor  $\sim 6$ . This implies that most of the stars have formed in a coherent starburst of the whole  $\sim 10^{11} M_{\odot}$  of gas in its late stages of collapse or assembly rather than in the smaller progenitors during the preceding period of hierarchical buildup. The implied suppression of SFR in small haloes and its possible origin will be discussed in §6.

The burst duration is also shorter than the characteristic time for cosmological accretion onto dark haloes of  $\sim 10^{12} M_{\odot}$ , the likely hosts of the  $M_d \sim 10^{11} M_{\odot}$  maximum bursters, as given by the inverse of the average  $\dot{M}/M$  in eq. (1). At  $z = 0.75$ , one has  $t_{\text{acc}}(10^{12} M_{\odot}) \simeq 7$  Gyr, much longer than the indicated observed duration of  $\Delta t \sim 1$  Gyr. At  $z = 2.4$ , one has  $t_{\text{acc}}(10^{12} M_{\odot}) \simeq 1.6$  Gyr, which is about 3 times the observed  $\Delta t \sim 0.5$  Gyr, though if the relevant haloes are more massive,  $\lesssim 10^{13} M_{\odot}$ , the accretion time is  $\sim 50\%$  shorter. As seen in Fig. 8, the burst durations are rather comparable to the shortest characteristic time of the system,  $t_{\text{vir}}$ .

Gas-rich *major mergers*, which could in principle produce such rapid, massive bursts, fail to match the robust features (a), (d) and (e). In particular, major mergers are expected to destroy the discs and be associated with perturbed clumpy morphology and kinematics rather than a smooth rotating disc. This is because the dynamical disturbance, involving tidal effects and violent relaxation, is expected to be pushed to an extreme during the  $\sim 100$  Myr of the close passages. Furthermore, the induced star formation is expected to be concentrated in a central cusp rather than an extended disc. It is worth noting that the mergers are only weakly associated with a characteristic mass, the nonlinear clustering scale  $M_*$ , which varies rapidly with time — they are not associated with galaxies of any specific fixed mass.

The SAMBA bursts, as described by our naive spherical model above, have the potential of reproducing the observed features one by one in a straightforward way. In particular, they have the potential of keeping the disc intact while doubling its mass and puffing up its thickness. This is because the disc buildup, even if it involves filamentary and clumpy cold flows, could be rather uniformly stretched over the  $\sim 0.5\text{--}1$  Gyr duration of the burst, and therefore involve only moderate perturbative effects on the dynamics. In addition, the SAMBA bursts are predicted to be specifically associated with one characteristic baryonic mass of  $\sim 10^{11} M_{\odot}$  at all redshifts.

The early SAMBA bursts, which may be associated with the observed maximum bursters at  $z \gtrsim 2$ , are predicted to be in  $M_d \sim 2 \times 10^{11} M_{\odot}$  discs embedded in rather massive haloes of  $M \sim 6 \times 10^{12} M_{\odot}$ . The comoving number density of haloes of  $M > 5 \times 10^{12} M_{\odot}$  at  $z = 2.2$  is  $n \simeq 10^{-4} (h^{-1} \text{Mpc})^{-3}$ , consistent with the number density of observed maximum bursters (Genzel et al.

2006)<sup>2</sup> The predicted halo virial velocity is  $\sim 400 \text{ km s}^{-1}$  and the virial radius is  $\sim 200 \text{ kpc}$ . The low concentration expected for such haloes at  $z \sim 2.2$ ,  $C \sim 4$  (Bullock et al. 2001), implies that the circular velocity at  $\sim 10 \text{ kpc}$  should be  $\sim 200 \text{ km s}^{-1}$ , compatible with the observed bursters. The large virial radius for that epoch, with an assumed typical spin parameter, implies an exponential disc radius of  $\sim 5 \text{ kpc}$  (Bullock et al. 2001), which explains the observed extended discs.

Thus, the burst properties predicted by the idealized spherical model do surprisingly well in matching the observed bursts.

#### 4.2 Suppressed Star Formation Rate

Despite the apparent vigor of the burst event, the most robust feature of the SAMBAs is the quenching. We note that during the SAMBA sequence of events, from the onset of the shock till the end of the burst about a Hubble time later, each galaxy spends more time in a phase of suppressed accretion rate rather than in a rapid accretion mode. Figure 9 shows a crude estimate of the predicted distribution of disc accretion rate for galaxies in the stellar mass bin  $(0.5-2) \times 10^{11} M_{\odot}$  near  $z \sim 2$ . This crude estimate is based on the fraction of time spent at each accretion rate in the simulated SAMBA shown in Fig. 3, assuming that it is a representative SAMBA at that epoch. While a fraction of the galaxies are expected to show a high accretion rate into the disc at about twice the average virial level, *more than half* the galaxies are predicted to present a strongly suppressed disc accretion rate, an order of magnitude below the virial accretion rate or less. The associated distribution of SFR may be qualitatively similar.

Preliminary indications for a substantial population of  $\sim 10^{11} M_{\odot}$  galaxies with strongly suppressed SFR already exist. A bimodality in the SFR distribution is apparent at  $z \lesssim 1$  in Noeske et al. (2007, Fig. 1), where the typical SFR is  $> 10 M_{\odot} \text{ yr}^{-1}$  while about half the galaxies have an upper limit of  $\text{SFR} < 1 M_{\odot} \text{ yr}^{-1}$ . At  $z \sim 2-2.7$ , Kriek et al. (2006) report that a significant fraction of the  $\sim 10^{11} M_{\odot}$  galaxies have surprisingly low upper limits for the specific SFR at  $< 0.1 \text{ Gyr}^{-1}$ , while the typical is  $\sim 1 \text{ Gyr}^{-1}$ .

The SAMBAs predict that the SFR histories of galaxies should show two peaks of SFR separated by a couple of Gyr, but this might be hard to detect observationally.

#### 4.3 Downsizing

The SAMBA phenomenon provides a simple explanation for the observed ‘‘downsizing’’ of elliptical galaxies. An ‘‘archaeological’’ analysis of stellar ages reveals that today’s more massive ellipticals have formed their

<sup>2</sup> This estimate is for the WMAP3 parameters of the  $\Lambda$ CDM cosmology,  $\Omega_m = 0.24$ ,  $\Omega_{\Lambda} = 0.76$ ,  $h = 0.73$ , and  $\sigma_8 = 0.74$  (Spergel et al. 2006). A similar number density is obtained for haloes twice as massive if one adopts instead  $\Omega_m = 0.3$ ,  $\Omega_{\Lambda} = 0.7$ ,  $h = 0.7$ , and  $\sigma_8 = 0.9$ .

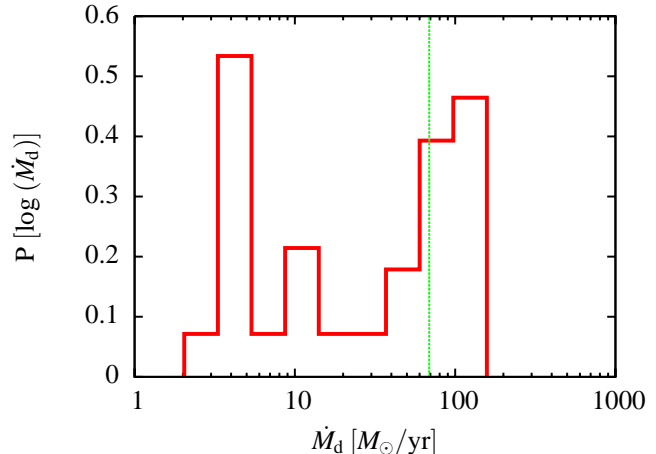


**Figure 9.** Predicted distribution of log disc accretion rate for galaxies in the disc-mass bin  $(0.5-2) \times 10^{11} M_{\odot}$  near  $z \sim 2$ . The vertical green line marks the mean virial accretion rate. About half the galaxies are expected to show a high accretion rate into the disc, while the other half is predicted to suffer a strongly suppressed accretion rate.

stars earlier and over a shorter time span (Thomas et al. 2005). From their SFR histories as a function of look-back time one learns that elliptical galaxies of present-day stellar mass  $\simeq 10^{11} - 10^{12} M_{\odot}$  have formed most of their stars at  $z \sim 2-3$  in a maximum burst over 1-0.5 Gyr with  $\dot{M}_d/M_d \sim 2$  (or  $z \sim 1.2-1.6$  in lower density environments). The progenitors of today’s ellipticals, prior to their subsequent growth via dry mergers, seem to be consistent with the maximum bursters seen at high redshift, and with the SAMBA predictions.

The constancy of  $M_{\text{sh}}$  with redshift, which implies that all galaxies burst when they are  $M_d \sim 10^{11} M_{\odot}$  and quench immediately after automatically implies downsizing in both the peak of SFR and the subsequent quenching. Galaxies of larger stellar mass today are likely to be embedded in more massive haloes, which in turn have crossed the threshold mass for the onset of SAMBA at an earlier time. They burst earlier, for a shorter duration, and shut down earlier accordingly. This is demonstrated in a cosmological semi-analytic simulation by Cattaneo et al. (2007).

The SAMBAs predict yet another kind of downsizing phenomenon, concerning halo mass at burst: the early bursts at  $z > 1.4$  are predicted to reside in massive haloes only slightly smaller than  $M \sim 10^{13} M_{\odot}$ , while the late bursts are to be found in smaller haloes,  $M \sim 10^{12} M_{\odot}$ .

## 5 RECIPES FOR SEMI-ANALYTIC MODELS

In order to study the potential observable implications of the SAMBA phenomenon in more detail, one can translate the predictions from the spherical model into a recipe for gas cooling and accretion rate onto the disc. This recipe is to be incorporated in Semi-Analytic Models (SAM), which follow the baryonic physics in given dark-halo merger trees. The SAMBA recipe should replace the standard recipe adopted in

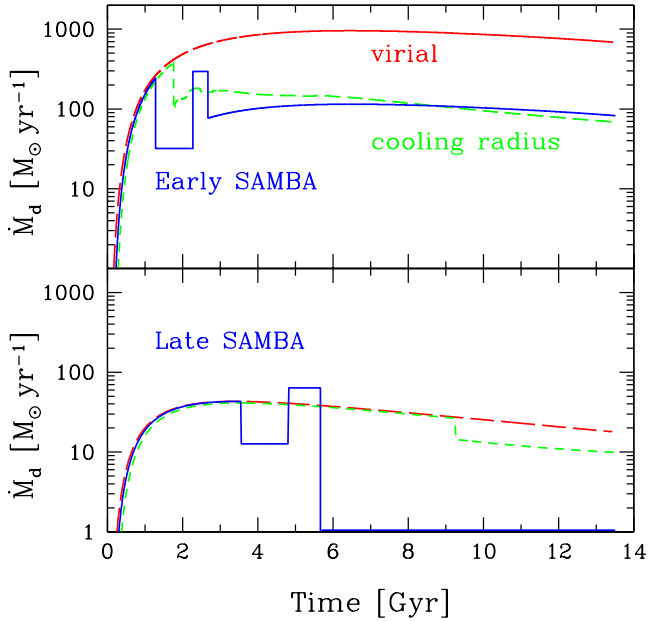


**Figure 10.** Disc growth rate in the SAMBA recipe for SAM (blue, solid) versus the smooth virial baryonic accretion rate (red, long dash) and the SAM standard (green, short dash) based on the evolution of the “cooling radius” a la White & Frenk (1991). **Top:** an early SAMBA ( $z_1 \simeq 4.8$ ,  $M_0 \simeq 10^{14} M_\odot$ ). In this case, long-term quenching has to originate from another process. **Bottom:** a late SAMBA ( $z_1 \simeq 1.8$ ,  $M_0 \simeq 4 \times 10^{12} M_\odot$ ), were long-term quenching is a natural outcome of uniform accretion.

SAMs (White & Frenk 1991), which assumes that the halo gas interior to a “cooling radius” is accreted onto the disc. The cooling radius within a (spherical) halo of a given mass at a given time is traditionally determined by the position where the cooling time equals a certain dynamical time, e.g., the Hubble time. The SAMBA phenomenon suggests a deterministic modification of the disc accretion rate, based on our spherical modeling, with no free parameters. However, an optimal match to observations may suggest a certain fine-tuning of the model parameters, compensating for deviations from spherical symmetry and uniform accretion.

### 5.1 Following Halo Evolution in SAM

The proposed SAMBA recipe for the accretion rate onto the disc is specified in §B1. In summary, given the mass growth of each halo in the merger tree,  $M(t)$ , and its derivative  $\dot{M}$ , the SAMBA onset time  $t_1$  (redshift  $z_1$ ) is identified by  $M(t_1) = M_1 = 10^{12} M_\odot$ , and the SAMBA is classified as “early type” or “late type” according to whether  $z_1 > 2.5$  or  $z_1 \leq 2.5$  respectively. Then the times  $t_2$  and  $t_3$ , the beginning and the end of the burst, are computed using the fits shown in Fig. 5. The algorithm then specifies the growth rates of cold and hot gas mass during each of the four SAMBA phases defined by the above times. The numerical factors used for the tentative quenching and for the burst are read from straightforward fits to  $\Delta M_d / (\Delta M f_b)$  in Fig. 7.

The disc mass growth according to the proposed

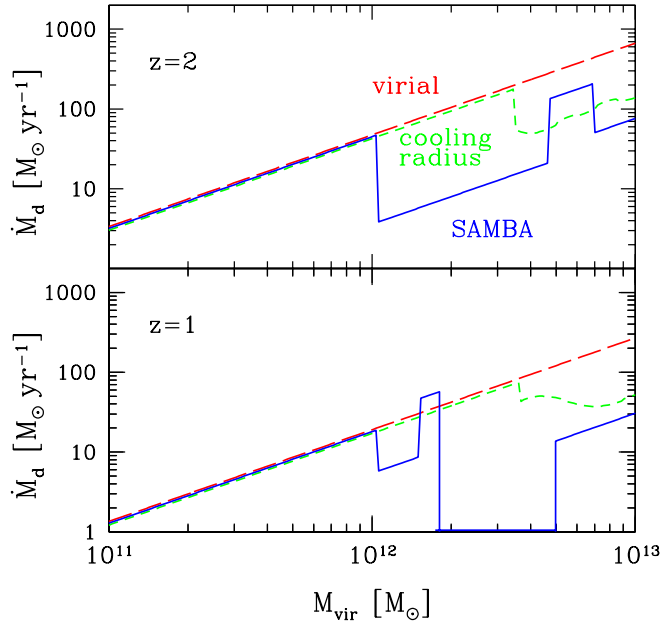


**Figure 11.** Disc growth in the SAMBA recipe for FHM (blue, solid) versus the virial baryonic accretion rate (red, long dash) and the standard based on “cooling radius” (green, short dash). **Top:** at  $z = 2$ . **Bottom:** at  $z = 1$ . Quenching in haloes  $\sim 10^{13} M_\odot$  and larger has to be due to another process.

SAMBA recipe for SAM is shown in Fig. 10 for typical early and late SAMBAs. It is compared to the standard disc growth rate following the evolution of a “cooling radius”. The latter has a characteristic drop when the cooling radius first becomes smaller than the virial radius. The cooling-radius recipe can be somewhat improved once the Hubble time used in its definition is replaced by  $t_{\text{vir}} = 0.18 t_{\text{Hubble}}$ . Yet, it fails to capture the depth of the tentative quenching, the burst, and the long-term quenching of late SAMBAs.

Recall that the early SAMBAs, ending up in  $M \geq 10^{13} M_\odot$  haloes today, should be quenched after  $t_3$  by another mechanism, such as clumpy accretion or AGN feedback. If such a process is not explicitly included in the SAM, one can simply set  $\dot{M}_d = 0$  in the post-burst phase for all haloes (as in Cattaneo et al. 2006).

### 5.2 SFR as a function of Halo Mass: FHM

An alternative, quick and crude way to learn about the implications of SAMBAs is by providing a recipe for the SFR as a function of halo mass and redshift, to be incorporated in a given halo population in a partial SAM while bypassing the detailed baryonic processes of cooling, star formation, and feedback (Formation History Modeling, FHM, Croton & Dekel 2007). The fact that the SAMBA phenomenon is driven by halo mass allows us to provide a concrete recipe of this sort, specified in §B2.

In summary, one starts with  $M_1 = 10^{12} M_\odot$  at  $t_1$ , and computes the other SAMBA characteristic halo masses  $M_2$  and  $M_3$ , corresponding to the characteristic times  $t_2$  and  $t_3$ , using fits to our simulation results.

Given the virial accretion rate in the provided merger tree,  $\dot{M}$ , the disc accretion rate, which could be interpreted as an upper limit for the SFR, is given in each of the mass ranges, corresponding to the four SAMBA phases. The numerical values are read from crude fits to the simulation results for  $\Delta M_d / (\Delta M f_b)$ , as shown in Fig. 7. When implementing the recipe, one can either use the actual mass growth rate of the haloes drawn from merger-tree realizations, or the average virial accretion rate as provided in eq. (3).

The SAMBA recipe for disc accretion rate is shown in Fig. 11, compared to the standard rate based on a “cooling radius”. Again, the cooling-radius recipe can be somewhat improved once the Hubble time is replaced by  $t_{\text{vir}}$ , but it would still fail to recover the burst and the deep quenching features of the SAMBAs.

The main feature of the SAMBA FHM is the quenching of SFR above a threshold halo mass,  $M_{\text{sh}} \sim 10^{12} M_{\odot}$ , as already implemented in SAM simulations (Cattaneo et al. 2006; Croton et al. 2006). The interesting new feature predicted by the model is the high SFR in a second range of masses above  $M_{\text{sh}}$ . At low redshifts, this is a slight increase of the effective threshold mass for quenching to  $\sim 2 \times 10^{12} M_{\odot}$ . At  $z \geq 1.3$ , the high SFR is predicted to extend to haloes as large as  $\sim 7 \times 10^{12} M_{\odot}$ . This should allow the appearance of massive blue galaxies at high redshifts. In the special range  $1.24 < z < 1.53$ , the high SFR is expected over an especially broad range of masses,  $1.5-7 \times 10^{12} M_{\odot}$  (not shown in Fig. 11). Given that  $10^{12} M_{\odot}$  is the typical mass for haloes that form at this redshift range, this should lead to a peak in the history of cosmological SFR density (the “Madau” plot).

## 6 DISCUSSION AND CONCLUSION

A straightforward spherical model of uniform gas accretion onto haloes predicts a robust, rich sequence of events in the accretion onto the central discs, SAMBA, which could be the major driver of star-formation history in galaxies. An initial *cold accretion* phase ends abruptly upon the birth of a shock in the inner regions of a halo once its mass exceeds a threshold mass of  $\sim 10^{12} M_{\odot}$  and the disc contains  $\sim 10^{11} M_{\odot}$ . The infall of gas through the expanding shock creates a period of *tentative quenching*, where the accretion onto the disc is suppressed for a couple of Gyr. The accumulating hot gas joins new incoming gas in a big crunch, leading to a massive, rapid, *burst* involving  $\sim 10^{11} M_{\odot}$  of gas in a few hundred Myr. The subsequent expansion of the shock to the virial radius results in a *long-term shutdown*, which is especially efficient if the burst occurs after  $z \sim 1.4$ , corresponding to today’s haloes of  $\lesssim 10^{13} M_{\odot}$ . The predicted SAMBA bursts seem to match the observed maximum bursters of  $M_d \sim 10^{11} M_{\odot}$  at  $z \lesssim 1$  and at  $z \gtrsim 2$ , as well as the indicated population of  $M_d \sim 10^{11} M_{\odot}$  galaxies with suppressed SFR. This rich phenomenon is a generic consequence of uniform accretion, before including the effects of major mergers or AGN feedback.

The implications of the SAMBA phenomenon should be taken with a grain of salt because the rel-

evance of the spherical uniform accretion model to the actual SFR history in real galaxies is yet to be demonstrated. This is an immediate challenge for cosmological simulations. The actual accretion could be rather filamentary and clumpy to begin with, and one should verify the extent to which the SAMBA behavior remains valid under such conditions. One could be encouraged though by the success of the spherical model in predicting the threshold mass for virial shock heating (Kereš et al. 2005; Dekel & Birnboim 2006; Birnboim et al. 2007). First clues for natural long-term quenching of the sort predicted here in a  $\sim 10^{12} M_{\odot}$  halo may be seen in high-resolution simulations of galaxies with quiet histories (Naab et al. 2007; Libeskind & Dekel 2007). The following discussion of possible implications is pursued under the tentative assumption that other robust SAMBA features will also be reproduced in cosmological simulations of the formation of such galaxies. The apparent match of the spherical predictions with several different observations makes this discussion worthwhile.

Using the fact that the accretion onto the disc is a straightforward function of halo mass, we propose a simple accretion recipe for SAMs, to replace the standard recipe based on a “cooling radius”. A realistic study of the SFR that is associated with this galaxy buildup, both in the case of smooth accretion of minor mergers and under major mergers and feedback effects, is necessary for a reliable comparison with observations. Still, the naive interpretation of the disc accretion rate as the maximum possible SFR provides a preliminary indication for a surprisingly good match to observations.

An obvious necessary condition for SAMBAs (which is actually automatically implied by the observed maximum bursts independent of any model) is that a substantial fraction of the accreting material onto haloes of  $\sim 10^{12} M_{\odot}$  is gaseous rather than stellar. Star formation could have been suppressed in haloes smaller than a certain threshold due to different processes, such as stellar feedback or a density threshold for star formation. Given such a threshold mass, we can estimate the gas fraction in the accretion by evaluating the mass in all accreting haloes below that threshold compared to the total accreting mass (Neistein & Dekel 2007). We find using the EPS formalism specified in §A that about one half of the accreting mass onto a halo of  $10^{12} M_{\odot}$  is in haloes smaller than  $\sim 10^{11} M_{\odot}$  (or “smooth” accretion), independent of time. This should therefore be the minimum halo mass for star formation in order to have a gas-dominated accretion. If the suppression is due to supernova feedback, the minimum mass for star formation corresponds to haloes of virial velocity  $\sim 120 \text{ km s}^{-1}$  (Dekel & Silk 1986; Dekel & Birnboim 2006, Fig. 2), for which the accretion is almost all gaseous at  $z = 0$ , it is about 90% at  $z \simeq 0.7$ , and about 67% at  $z \simeq 2.4$ . This hints that supernova feedback could be the suppression mechanism allowing the accretion onto  $\sim M_{\text{sh}}$  haloes to be predominantly gaseous at all relevant redshifts.

The dramatic variations in the disc accretion rate imply that each galaxy is likely to evolve through several subsequent phases of very high and very low SFR. This means that the expected overall trend of evolution

from the blue cloud to the red sequence of galaxies is not a one-way track. In particular, some of the red & dead galaxies observed at high redshift may actually become blue again at later redshifts. The lesson is that the interpretation of the observed evolution of the blue and red luminosity functions may involve non-trivial book-keeping.

The late SAMBAs offer a very efficient post-burst shutdown that lasts for 6-7 Gyr. This can naturally give rise to red & dead galaxies in today's small-group haloes of  $\leq 10^{13} M_{\odot}$ , perhaps S0 or elliptical galaxies (as simulated by Naab et al. 2007; Libeskind & Dekel 2007).

In the early SAMBAs, the accretion rate into the disc is suppressed compared to the virial rate even during the burst phase, but the post-burst accretion rate is not negligible. For these central galaxies in today's cluster haloes of  $> 10^{13} M_{\odot}$  to end up as large red & dead ellipticals one needs a quenching mechanism beyond the one provided by spherical accretion. We show elsewhere (Birnboim & Dekel 2007) that this could be provided by clumpy accretion, in which gas clumps of  $10^7 - 10^9 M_{\odot}$  transfer their gravitational energy via drag and local shocks into heating and puffing up of the inner-halo gas of  $\geq 10^{13} M_{\odot}$  haloes.

Alternatively, a fashionable scenario suggests that the required quenching is provided by AGN feedback (Croton et al. 2006; Cattaneo et al. 2006). It has been noticed that the shock heating of the gas in haloes  $> 10^{12} M_{\odot}$  enables the required coupling of the AGN energy with the halo gas (Dekel & Birnboim 2006), but we now realize that the SAMBA burst may be the actual trigger for AGN activity just above this critical mass. The SAMBAs may thus be responsible for both, the energy source and the coupling mechanism.

If the SAMBAs are responsible for triggering AGN activity, recall that they do so only in galaxies of  $\sim 10^{11} M_{\odot}$ , a couple of Gyr after their haloes became larger than  $\sim 10^{12} M_{\odot}$ . This may explain the otherwise surprising result that the bright quasars (near  $L_{*}$  of their Schechter luminosity function) seem to reside at all redshifts in haloes of  $\sim 2 \times 10^{12} M_{\odot}$  (Croom et al. 2005). A straightforward calculation using the Press-Schechter formalism shows that the evolution of number density of quasars at  $z > 1$  can be reproduced by assuming quasar onset in every halo when it first becomes  $\sim 2 \times 10^{12} M_{\odot}$  and allowing a fixed short lifetime for each quasar.

The SAMBA events offer a complementary alternative to wet major mergers in producing rapid, massive bursts, with the important difference that it can leave the disc intact. The associated shutdown leads to red & dead galaxies in haloes above the threshold mass. However, while major mergers also automatically produce spheroids, what could be the mechanism responsible for spheroid formation in association with the old, gas-poor stellar population according the halo shutdown scenario? First, the SAMBA burst provides the gas necessary for bar instability in the disc, which then transfers angular momentum to the outer disc and halo and produces a bulge. Second, the SAMBA quenching makes any subsequent mergers dryer, so they could lead to the large, boxy, non-rotating ellipticals, which cannot be re-

produced by wet major mergers (Novak & et al., 2007). Third, the minor mergers associated with the continuous smooth accretion of SAMBA could themselves lead to the formation of a spheroid (Naab et al. 2007; Bourneaud & et al., 2007; Libeskind & Dekel 2007).

We argued in Dekel & Birnboim (2006) that discs could be built and form stars by cold streams, which could persist as narrow filaments even within the shock heated medium slightly above  $M_{\text{sh}}$ , especially at high redshifts. Streaming at the virial velocity, these flows could indeed give rise to rapid starbursts, on a time scale comparable to the virial crossing time, but it is not clear that these flows could bring in mass in a rate that is much more efficient than the cosmological accretion rate. The SAMBAs provide such more efficient bursts in a natural way.

All the above is yet to be confirmed in cosmological simulations. It would be interesting to learn how the SAMBA phenomenon manifests itself when the spherical accretion of minor mergers is accompanied by filamentary streams and major mergers.

## ACKNOWLEDGMENTS

We acknowledge stimulating discussions with S.M. Faber, R. Genzel, F. Hammer & J.P. Ostriker. This research has been supported by ISF 213/02 and GIF I-895-207.7/2005.

## REFERENCES

- Bardeen J. M., Bond J. R., Kaiser N., Szalay A. S., 1986, ApJ, 304, 15
- Binney J., 1977, ApJ, 215, 483
- Binney J., 2004, MNRAS, 347, 1093
- Birnboim Y., Dekel A., 2003, MNRAS, 345, 349
- Birnboim Y., Dekel A., 2007, in preparation
- Birnboim Y., Dekel A., Kravtsov A., Zinger E., 2007, in preparation
- Blumenthal G. R., Faber S. M., Primack J. R., Rees M. J., 1984, Nature, 311, 517
- Bourneaud F., et al., 2007, PhD thesis, IAP, Paris
- Bullock J. S., Dekel A., Kolatt T. S., Kravtsov A. V., Klypin A. A., Porciani C., Primack J. R., 2001, ApJ, 555, 240
- Bullock J. S., Kolatt T. S., Sigad Y., Somerville R. S., Kravtsov A. V., Klypin A. A., Primack J. R., Dekel A., 2001, MNRAS, 321, 559
- Cattaneo A., Dekel A., Devriendt J., Guiderdoni B., Blaizot J., 2006, MNRAS, 370, 1651
- Cattaneo A., Dekel A., Faber S. M., 2007, astro-ph/07xxxx
- Croom S. M., Boyle B. J., Shanks T., Smith R. J., Miller L., Outram P. J., Loaring N. S., Hoyle F., da Ângela J., 2005, MNRAS, 356, 415
- Croton D. J., Dekel A., 2007, astro-ph/07xxxx
- Croton D. J., Springel V., White S. D. M., De Lucia G., Frenk C. S., Gao L., Jenkins A., Kauffmann G., Navarro J. F., Yoshida N., 2006, MNRAS, 365, 11
- Dekel A., Birnboim Y., 2006, MNRAS, 368, 2

Dekel A., Silk J., 1986, *ApJ*, 303, 39  
 Förster Schreiber N. M., Genzel R., Lehnert M. D., Bouché N., Verma A., Erb D. K., Shapley A. E., et al., 2006, *ApJ*, 645, 1062  
 Genzel R., Tacconi L. J., Eisenhauer F., Förster Schreiber N. M., Cimatti A., Daddi E., Bouché N., et al., 2006, *Nature*, 442, 786  
 Hammer F., Flores H., Elbaz D., Zheng X. Z., Liang Y. C., Cesarsky C., 2005, *A&A*, 430, 115  
 Kereš D., Katz N., Weinberg D. H., Davé R., 2005, *MNRAS*, 363, 2  
 Kravtsov A. V., 2003, *ApJ*, 590, L1  
 Kravtsov A. V., Gnedin O. Y., 2005, *ApJ*, 623, 650  
 Kriek M., van Dokkum P. G., Franx M., Quadri R., Gawiser E., Herrera D., Illingworth G. D., et al., 2006, *ApJ*, 649, L71  
 Lacey C., Cole S., 1993, *MNRAS*, 262, 627  
 Libeskind N., Dekel A., 2007, in preparation  
 Lotz J. M., Davis M., Faber S. M., Guhathakurta P., Gwyn S., Huang J., Koo D. C., et al., 2006, *astro-ph/0602088*  
 Mo H. J., White S. D. M., 2002, *MNRAS*, 336, 112  
 Naab T., Johansson P. H., Efstathiou G., Ostriker J. P., 2007, *astro-ph/0512235*  
 Neistein E., Dekel A., 2007, in preparation  
 Neistein E., van den Bosch F. C., Dekel A., 2006, *MNRAS*, 372, 933  
 Noeske K. G., Weiner B. J., Faber S. M., Papovich C., Koo D. C., Somerville R. S., Bundy K., Conselice C. J., et al., 2007, *astro-ph/0701924*  
 Novak G., et al., 2007, in preparation  
 Rees M. J., Ostriker J. P., 1977, *MNRAS*, 179, 541  
 Silk J., 1977, *ApJ*, 211, 638  
 Spergel D. N., Bean R., Doré O., Nolta M., Bennett C. L., Hinshaw G., Jarosik N., et al., 2006, *astro-ph/0603449*  
 Sugiyama N., 1995, *ApJS*, 100, 281  
 Sutherland R. S., Dopita M. A., 1993, *ApJS*, 88, 253  
 Thomas D., Maraston C., Bender R., de Oliveira C. M., 2005, *ApJ*, 621, 673  
 van den Bosch F. C., 2002, *MNRAS*, 331, 98  
 Wechsler R. H., Bullock J. S., Primack J. R., Kravtsov A. V., Dekel A., 2002, *ApJ*, 568, 52  
 White S. D. M., Frenk C. S., 1991, *ApJ*, 379, 52  
 White S. D. M., Rees M. J., 1978, *MNRAS*, 183, 341

## APPENDIX A: MAIN PROGENITOR HISTORY

Following Neistein et al. (2006), we use the EPS formalism (Lacey & Cole 1993) to derive an analytic estimate for the main progenitor history. We track time backwards via the variable  $\omega = \delta_c/D(t)$ , where  $D(t)$  is the cosmological growth factor of linear density fluctuations normalized to  $D(t_0) = 1$  (see below), and  $\delta_c \simeq 1.68$  (ignoring small variations due to the actual cosmology used). Mass enters via the monotonically decreasing function  $\sigma(M)$ , the standard deviation of the initial density fluctuations, as derived from their power spectrum, smoothed on a scale that corresponds to mass  $M$  and linearly extrapolated to  $t_0$  (see below). According to EPS, a halo of mass  $M_0$  at  $\omega_0$  has the following average number of progenitors of mass in the range  $(M, M + dM)$  at the earlier time  $\omega_0 + \Delta\omega$ :

$$dN = \frac{1}{\sqrt{2\pi}} \frac{\Delta\omega}{(\Delta\sigma^2)^{3/2}} \exp\left[-\frac{(\Delta\omega)^2}{2\Delta\sigma^2}\right] \left| \frac{d\sigma^2}{dM} \right| \frac{M_0}{M} dM, \quad (\text{A1})$$

where  $\Delta\omega = \omega - \omega_0$  and  $\Delta\sigma^2 = \sigma^2(M) - \sigma^2(M_0)$ .

### A1 Accretion Rate onto $M$ at $t$ : a Small Time Step

We wish to compute the main progenitor history, i.e., the conditional average  $M(\omega|\omega_0, M_0)$ . The main progenitor is guaranteed to also be the most massive progenitor when  $\Delta\omega$  is small enough, and this allows us to compute  $\dot{M}$  by evaluating  $M(\omega_0 + \Delta\omega|\omega_0, M_0)$  for small  $\Delta\omega$ .

For  $M \geq M_0/2$ , the probability density  $P(M, \omega|M_0, \omega_0)$  is the same as the total progenitor distribution  $dN/dM$  given by equation A1. For  $M < M_0/2$ , however, the only condition is  $P \leq dN/dM$ , and it is not sufficient to constrain  $P$ . As a first approximation we assume that the main progenitor always has a mass  $M \geq M_0/2$ . Then, the average mass of the main progenitor is

$$M(\omega_0 + \Delta\omega|\omega_0, M_0) = \int_{M_0/2}^{M_0} \frac{dN}{dM} M dM \quad (\text{A2})$$

$$= M_0 \left[ 1 - \text{erf} \left( \frac{\Delta\omega}{\sqrt{2\sigma_q^2 - 2\sigma_0^2}} \right) \right],$$

where  $\sigma_q = \sigma(M_0/q)$  with  $q = 2$ , and  $\sigma_0 = \sigma(M_0)$ . The rate of change is then

$$\frac{dM}{d\omega} = \lim_{\Delta\omega \rightarrow 0} \frac{M(\omega_0 + \Delta\omega|\omega_0, M_0) - M_0}{\Delta\omega} \quad (\text{A3})$$

$$= -M_0 \lim_{\Delta\omega \rightarrow 0} \frac{1}{\Delta\omega} \text{erf} \left( \frac{\Delta\omega}{\sqrt{2\sigma_q^2 - 2\sigma_0^2}} \right).$$

Using the limit  $\text{erf}(x) \rightarrow 2x/\sqrt{\pi}$  when  $x \rightarrow 0$  we get

$$\frac{1}{M} \frac{dM}{d\omega} = - \left( \frac{2/\pi}{\sigma_q^2 - \sigma_0^2} \right)^{1/2}. \quad (\text{A4})$$

Thus, the mean specific accretion rate onto haloes of mass  $M$  at  $t$  is

$$\frac{\dot{M}}{M} (M, t) = -s(M) \dot{\omega}(t), \quad (\text{A5})$$

with

$$s(M) \equiv \left[ \frac{2/\pi}{\sigma^2(M/q) - \sigma^2(M)} \right]^{1/2}, \quad (\text{A6})$$

$$\dot{\omega}(t) = -\frac{\delta_c}{D} \frac{\dot{D}}{D}. \quad (\text{A7})$$

When  $\Delta\omega$  is not negligibly small, the probability for  $M < M_0/2$  is not negligible, as it grows in proportion to  $\Delta\omega$ . Neistein et al. (2006) showed that this effect is rather small and can be bounded by well defined limits

on  $q$ , though the exact value of  $q$  is not fully specified by the EPS formalism. They showed that eq. (A5) is still a valid approximation, but with  $q$  slightly larger than 2, and limited to the range 2–2.3 for a flat  $\Lambda$ CDM cosmology with  $0.1 < \Omega_m < 0.9$  and  $10^8 < M < 10^{15} M_\odot$ . We adopt  $q = 2.2$  for all practical purposes.

As a sanity check, note that the obtained specific accretion rate at a fixed mass is self-similar in time, consistent with the fact that the only relevant mass scale at any given time is the non-linear clustering mass of the Press-Schechter formalism,  $M_*$ , defined by  $\sigma[M_*(t)] = \delta_c/D(t)$ . This is because the time dependence in eq. (A5) is via  $\dot{\omega} = -\sigma[M_*(t)]\dot{D}/D$ . Once  $\dot{M}/M$  is divided by the universal growth rate  $\dot{D}/D$ , the time dependence enters only through  $M_*(t)$ . Any viable approximation for the cosmological accretion rate must obey a self-similarity of this sort.

We also note in eq. (2) that at a fixed  $t$ ,  $\dot{M}/M \rightarrow \infty$  when  $M \rightarrow \infty$ , but recall that haloes of  $M \gg M_*$  are rare, such that most of the accreted mass is not onto arbitrarily massive haloes.

## A2 Mass Growth History of $M_0$ at $t_0$

The mass growth history of the main progenitor of a halo of mass  $M_0$  at  $t_0$  is obtained by integrating eq. (A4) over  $d\omega$  and over  $dM$  in the two sides of the equation:

$$\omega - \omega_0 = F(M) - F(M_0), \quad F(M) \equiv \int_M^\infty \frac{dm}{m s(m)}. \quad (\text{A8})$$

The desired average mass of the main progenitor at  $t$  can be extracted from the above equation,

$$M(t|M_0) = F^{-1}[\omega - \omega_0 + F(M_0)], \quad w = \frac{\delta_c}{D(t)}, \quad (\text{A9})$$

where  $F^{-1}$  is the inverse function of  $F$ , to be evaluated either explicitly or via numerical interpolation.

## A3 A Power-Law Power Spectrum

A simple, fully self-similar example is provided by a power-law power spectrum,  $P_k \propto k^n$ , for which

$$\sigma = \sigma_R M^{-\alpha}, \quad \alpha \equiv (n+3)/6. \quad (\text{A10})$$

Here  $\sigma_R$  is a normalization constant, and  $M$  is measured in units of  $M_R$ , the average mass originally contained in a top-hat sphere of comoving radius  $R$  (e.g.  $\sigma_8$  for  $R = 8 h^{-1} \text{Mpc}$ ). In this case, the average accretion rate is given by eq. (A5) with

$$s(M) = \tau M^\alpha, \quad \tau \equiv \frac{1}{\sigma_R} \left( \frac{2/\pi}{q^{2\alpha} - 1} \right)^{1/2}. \quad (\text{A11})$$

Then,

$$F(M) = \frac{1}{\alpha \tau} (M^{-\alpha} - M_0^{-\alpha}), \quad (\text{A12})$$

and the explicit solution for the average main-progenitor mass is

$$M(t|M_0) = [M_0^{-\alpha} + \alpha \tau (\omega - \omega_0)]^{-1/\alpha} \quad (\text{A13})$$

(with  $\omega = \delta_c/D(t)$ ,  $M$  in units of  $M_R$ , and  $q \simeq 2.2$ ).

Eq. (A5) with  $s(M)$  from eq. (A11) approximates the accretion rate for a general power spectrum once  $\alpha$  is the local slope  $\alpha(M) \equiv -d \ln \sigma / d \ln M$ . For  $n = -2.1$ , appropriate for  $M \sim 10^{12} M_\odot$  in the  $\Lambda$ CDM cosmology, we have  $\alpha \simeq 0.15$ . This is indeed similar to the power index of the mass dependence from N-body simulations (Wechsler et al. 2002, Fig. 12).

The time dependence can be approximated in standard  $\Lambda$ CDM by eq. (A29). Using a crude power-law approximation for the growth of the Press-Schechter mass out to  $z \sim 2$ ,  $M_*(z)/M_{*0} \simeq (1+z)^{-5}$ , we end up with a practical approximation for the accretion rate into haloes in the vicinity of  $M \sim 10^{12} M_\odot$ ,

$$\frac{\dot{M}}{M} \simeq 0.04 \text{Gyr}^{-1} (1+z)^{2.25} M_{12}^{0.15}, \quad (\text{A14})$$

which is accurate to better than 10% over the range  $0 \leq z \leq 2$ .

## A4 $\Lambda$ CDM Power Spectrum

For the standard  $\Lambda$ CDM power spectrum we adopt  $P(k) = k T^2(k)$  with the transfer function (Bardeen et al. 1986)

$$T(k) = \frac{\ln(1+2.34\kappa)}{2.34\kappa} \times [1 + 3.89\kappa + (16.1\kappa)^2 + (5.46\kappa)^3 + (6.71\kappa)^4]^{-1/4}. \quad (\text{A15})$$

Here  $\kappa \equiv k/\Gamma$ , with the wave number  $k$  in units of  $(h^{-1} \text{Mpc})^{-1}$ , and with the shape parameter  $\Gamma$  (Sugiyama 1995)

$$\Gamma = \Omega_m h \exp \left[ -\Omega_b (1 + \sqrt{2h}/\Omega_m) \right]. \quad (\text{A16})$$

This power spectrum can be used to derive  $\sigma(M)$  and the corresponding  $s(M)$  with  $q = 2.2$  in eq. (2). This can then be substituted in eq. (A5) for an explicit estimate of the average accretion rate onto haloes of mass  $M$  at  $t$ . It can then be used in eq. (A8) for computing  $F(M)$ , evaluating its inverse function numerically, and using it in eq. (4) to obtain the average history of the main progenitor,  $M(t|M_0)$ .

Alternatively, following van den Bosch (2002), the rms fluctuation corresponding the  $\Lambda$ CDM power spectrum is approximated (to better 1% in the range  $10^6 < M < 10^{16} M_\odot$ ) by

$$\sigma(M) = \sigma_8 \frac{\Psi[(M/M_c)^{1/3}]}{\Psi[32\Gamma]}, \quad (\text{A17})$$

$$M_c = 9.73 \times 10^{11} M_\odot h_{0.7}^{-1} (\Omega_m/0.3) (\Gamma/0.2)^{-3}, \quad (\text{A18})$$

and with the fitting function

$$\Psi(x) = 64.09 (1 + 1.074 x^{0.3} - 1.581 x^{0.4} + 0.954 x^{0.5} - 0.185 x^{0.6})^{-10}. \quad (\text{A19})$$

Substituting this analytic approximation in eq. (A8), numerically inverting  $F(M)$ , and using it in eq. (4), Neistein et al. (2006) derived the following approximation for the average main progenitor history:

$$\frac{M(t|M_0)}{M_c} = F_q^{-1} \left[ \frac{\Psi(32\Gamma)}{\sigma_8} (\omega - \omega_0) + F_q \left( \frac{M_0}{M_c} \right) \right], \quad (\text{A20})$$

with  $q = 2.2$  and the fitting function

$$F_{2.2}(u) = -6.92 \times 10^{-5} (\ln u)^4 + 5.0 \times 10^{-3} (\ln u)^3 + 8.64 \times 10^{-2} (\ln u)^2 - 12.66 (\ln u). \quad (\text{A21})$$

This fitting function is accurate to better than 1% over the range  $10^6 < M < 10^{15} M_\odot$  for the standard  $\Lambda$ CDM cosmology.

## A5 In Cosmological N-body Simulations

Wechsler et al. (2002) analyzed an N-body simulation of  $\Lambda$ CDM for the average mass-growth history of the main progenitor of a halo of mass  $M_0$  at  $t_0$ . They found a good fit with

$$M(t|M_0) = M_0 e^{-2a_c z}, \quad (\text{A22})$$

$$a_c = 0.28 \left( \frac{M_0}{10^{12} M_\odot} \right)^{0.15}. \quad (\text{A23})$$

This function is a good practical approximation to the EPS estimate specified above, as long as  $t_0$  is the present time,  $z = 0$ .

## A6 Useful Relations for Linear Fluctuations

Following Mo & White (2002), in a flat universe

$$D(z) = \frac{g(z)}{g(0)} \frac{1}{(1+z)}, \quad (\text{A24})$$

$$g(z) \simeq \frac{5}{2} \left( \Omega_m^{-3/7}(z) + \frac{3}{2} \right)^{-1}, \quad (\text{A25})$$

with a negligible error on the order of  $\Omega_\lambda/70$  in  $g(z)$ . Thus

$$\frac{\dot{D}}{D} \simeq H(z) \left( 1 + \frac{18}{35} g(z) \Omega_m^{-3/7}(z) [\Omega_m(z) - 1] \right). \quad (\text{A26})$$

Here

$$H(z) = H_0 E(z), \quad \Omega_m(z) = \frac{\Omega_{m0}(1+z)^3}{E^2(z)}, \quad (\text{A27})$$

$$E^2(z) = 1 - \Omega_{m0} + \Omega_{m0}(1+z)^3. \quad (\text{A28})$$

For  $\Lambda$ CDM with  $\Omega_m = 0.3$  and  $\Omega_\Lambda = 0.7$ , a practical approximation is

$$\frac{\dot{D}}{D} \simeq 0.0385 (1+z)^{3/2} h_{0.7} \text{Gyr}^{-1}, \quad (\text{A29})$$

which is accurate to better than 1% at  $z \geq 1$  and better than 10% at  $z \geq 0$ .

The fluctuation variance is derived in the general case by integrating the power spectrum,

$$\sigma^2(M) = \frac{1}{2\pi} \int_0^\infty dk k^2 P(k) \tilde{W}^2(kR), \quad (\text{A30})$$

with  $M = (4\pi/3)\rho_0 R^3$ , and with the Fourier transform of the real-space top-hat window function or radius  $R$

$$\tilde{W}(x) = 3(\sin x - x \cos x)/x^3. \quad (\text{A31})$$

## APPENDIX B: RECIPES FOR SAMs

### B1 Following Halo Evolution in SAM

Given the mass growth of each halo in the merger tree,  $M(t)$ , the SAMBA onset time  $t_1$  (redshift  $z_1$ ) is identified by  $M(t_1) = M_1 = 10^{12} M_\odot$ . The SAMBA is classified as “early type” or “late type” according to whether  $z_1 > 2.5$  or  $z_1 \leq 2.5$  respectively. Then the beginning and the end of the burst, as read from Fig. 5, are

$$t_2 = \begin{cases} 1.80 t_1, & z_1 > 2.5 \\ 1.36 t_1, & z_1 \leq 2.5 \end{cases}, \quad t_3 = 1.18 t_2. \quad (\text{B1})$$

This defines the four phases of gas cooling.

The growth rates of cold and hot gas mass during each phase can be approximated as follows:

1. **Cold-flow** phase,  $t \leq t_1$ ,

$$\dot{M}_d = f_b \dot{M}, \quad \dot{M}_{\text{hot}} = 0. \quad (\text{B2})$$

2. **Tentative-quenching** phase,  $t_1 < t \leq t_2$ ,

$$\dot{M}_d = f_b \frac{\Delta M_{12}}{\Delta t_{12}} \times \begin{cases} 0.08, & z_1 > 2.5 \\ 0.3, & z_1 \leq 2.5 \end{cases}, \quad (\text{B3})$$

$$\dot{M}_{\text{hot}} = f_b \dot{M} - \dot{M}_d, \quad (\text{B4})$$

where  $\Delta M_{ij} = M(t_j) - M(t_i)$  and  $\Delta t_{ij} = t_j - t_i$ . The numerical factors for early and late SAMBAs, both for the tentative quenching and for the burst below, are read from straightforward fits to  $\dot{M}_d/(\Delta M f_b)$  in Fig. 7.

3. **Burst** phase,  $t_2 < t \leq t_3$ ,

$$\dot{M}_d = f_b \frac{\Delta M_{23}}{\Delta t_{23}} \times \begin{cases} 0.5, & z_1 > 2.5 \\ 1.6, & z_1 \leq 2.5 \end{cases}, \quad (\text{B5})$$

$$\dot{M}_{\text{hot}} = -\frac{M_{\text{hot}2}}{\Delta t_{23}}, \quad (\text{B6})$$

where  $M_{\text{hot}2}$  is the accumulated hot gas mass by  $t_2$ ,  $M_{\text{hot}2} = f_b \Delta M_{12} - \dot{M}_{\text{disc},2} \Delta t_{12}$ . The cold accretion is more efficient in the late bursts because of the tentative shock instability due to the lower virial accretion rate at late times.

4. **Post-burst** phase,  $t > t_3$ ,

$$\dot{M}_d = f_b \dot{M} \times \begin{cases} 0.12, & z_1 > 2.5 \\ 0, & z_1 \leq 2.5 \end{cases}, \quad (\text{B7})$$

$$\dot{M}_{\text{hot}} = f_b \dot{M} - \dot{M}_d. \quad (\text{B8})$$

The numerical factor for early SAMBAs is read from the fit  $M/M_d \simeq 4/f_b$  at to the results shown in Fig. 7, combined with the fact, seen in Fig. 4, that during the post-burst phase  $\dot{M}_d/M_d \simeq \dot{M}/M$  and  $M/M_d \simeq \text{const}$ . Recall that the early SAMBAs, ending up in  $M \geq 10^{13} M_\odot$  haloes today, should be quenched after  $t_3$  by another mechanism, such as clumpy accretion or AGN feedback. If such a process is not explicitly included in the SAM, one can simply set  $\dot{M}_d = 0$  in the post-burst phase for all haloes (as in Cattaneo et al. 2006).

The disc mass growth according to the proposed SAMBA recipe for SAM is shown in Fig. 10, in comparison with the standard disc growth following the evolution of a “cooling radius”.

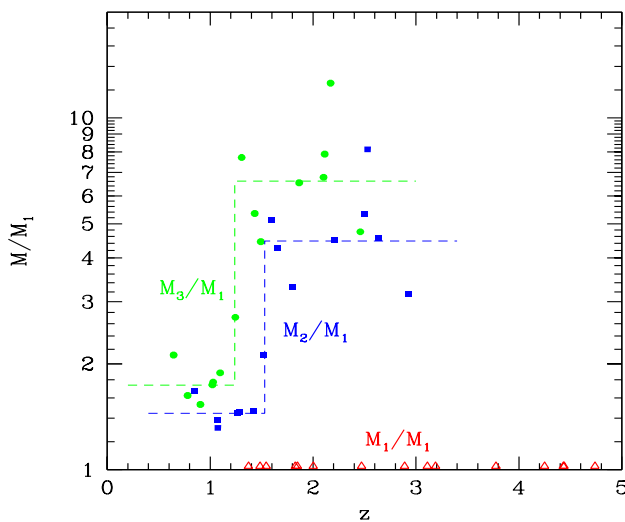


**Figure B1.** The characteristic SAMBA masses relative to  $M_1 \simeq 10^{12} M_\odot$ . Open red triangles refer to  $z_1$ . Solid blue squares refer to  $M_2/M_1$  at  $z_2$ . Solid green circles refer to  $M_3/M_1$  at  $z_3$ . The lines mark the fits used for the FHM recipe.

## B2 SFR as a function of Halo Mass: FHM

An alternative, quick and crude way to learn about the implications of SAMBAs is by providing a recipe for the SFR as a function of halo mass and redshift, to be incorporated in a given halo population in a SAM while bypassing the detailed baryonic processes of cooling, star formation, and feedback (Formation History Modeling, FHM, Croton & Dekel 2007). The fact that the SAMBA phenomenon is driven by halo mass allows us to provide a concrete recipe of this sort.

The SAMBA characteristic halo masses  $M_1$ ,  $M_2$  and  $M_3$ , corresponding to the characteristic times  $t_1$ ,  $t_2$  and  $t_3$ , can be approximated based on our simulations by

$$M_1 = 10^{12} M_\odot, \quad (B9)$$

$$M_2/M_1 = \begin{cases} 4.45, & z > 1.53 \\ 1.45, & z \leq 1.53 \end{cases}, \quad (B10)$$

$$M_3/M_1 = \begin{cases} 6.61, & z > 1.24 \\ 1.74, & z \leq 1.24 \end{cases}. \quad (B11)$$

The constant value of  $M_1$  is as predicted by Dekel & Birnboim (2006) for a realistic gradual increase of metallicity with time. Then  $M_2$  and  $M_3$  are obtained from the fits shown in Fig. B1. Notice the interesting prediction that in the range  $1.24 < z \leq 1.53$   $M_3$  is much larger than  $M_2$ , giving rise to a broad range of massive haloes with high SFR.

Given the virial accretion rate in the provided merger tree,  $\dot{M}$ , the disc accretion rate, which could be interpreted as an upper limit for the SFR, is approximated in the different mass ranges by:

1. **Cold-flow** range,  $M \leq M_1$ ,

$$\dot{M}_d = f_b \dot{M}. \quad (B12)$$

2. **Tentative-quenching** range,  $M_1 < M \leq M_2$ ,

$$\dot{M}_d = f_b \dot{M} \times \begin{cases} 0.08, & z > 1.8 \\ 0.3, & z \leq 1.8 \end{cases}. \quad (B13)$$

3. **Burst** range,  $M_2 < M \leq M_3$ ,

$$\dot{M}_d = f_b \dot{M} \times \begin{cases} 0.5, & z > 1.4 \\ 1.6, & z \leq 1.4 \end{cases}. \quad (B14)$$

The numerical values are read from crude fits to the simulation results for  $\Delta M_d / (\Delta M f_b)$ , as shown in Fig. 7.

4. **Post-burst** range,  $M > M_3$ ,

$$\dot{M}_d = f_b \dot{M} \times \begin{cases} 0.12, & M > M_q(z) \\ 0, & M \leq M_q(z) \end{cases}, \quad (B15)$$

$$M_q(z) \simeq 10^{13} M_\odot \exp(-0.75 z). \quad (B16)$$

The upper-limit for effective quenching,  $M_q(z)$ , is the mass of the intermediate SAMBA separating late from early SAMBAs, which eventually ends up as  $M = 10^{13} M_\odot$  today. The above estimate is based on the fit to simulations, eq. (A22). Note that once  $z > 1.4$ ,  $M_3 > M_q(z)$ , so in this redshift range  $M > M_3$  automatically implies  $M > M_q$ .

The numerical values in the quenching and burst phases are read from the crude fits to the simulation results shown in Fig. 7, in most of which the virial mass grows according to the average cosmological rate. When implementing the above recipe, one can either use the actual mass growth rate of the haloes drawn from merger-tree realizations, or the average virial accretion rate as provided in eq. (3).

The main feature of the model is the quenching of SFR above a threshold halo mass,  $M_{sh} \sim 10^{12} M_\odot$ , as already implemented in SAM simulations (Cattaneo et al. 2006; Croton et al. 2006). The interesting new feature predicted by the model is the high SFR in a second range of masses above  $M_{sh}$ . At low redshifts, this is a slight effective increase of the threshold mass to  $\sim 2 \times 10^{12} M_\odot$ . At  $z \geq 1.3$ , the high SFR is predicted to extend to haloes as large as  $\sim 7 \times 10^{12} M_\odot$ . This should allow the appearance of massive blue galaxies at high redshifts. In the special range  $1.24 < z < 1.53$ , the high SFR is expected over an especially broad range of masses. Given that  $10^{12} M_\odot$  is the typical mass for haloes that form at this redshift range, this should lead to a peak in the history of cosmological SFR density (the ‘‘Madau’’ plot).

## B3 Fine-tuning of the SAMBA Recipes

While the above recipes are our best guess based on the spherical model, with no free parameters, a better match to observations may require modest fine-tuning of model parameters, e.g., allowing for certain uncertainties in the assumptions made in the computations, as well as compensating for deviations from spherical symmetry and uniform accretion.

The uncertainty in the value of the critical mass for shock heating,  $M_{sh}$ , can easily accommodate a factor of two and some redshift dependence. As computed in Dekel & Birnboim (2006), it is a function of certain physical parameters, in particular redshift  $z$  and the average metallicity  $Z$  and gas fraction  $f_b$  in the inner

halo, which also vary with  $z$ . The estimates of  $M_{\text{sh}}$  as a function of  $z$  are shown in their figure 2. A practical approximation based on their equation 34 is

$$M_{\text{sh}} \simeq 10^{12} M_{\odot} \frac{Z_{0.2}^{0.52} f_{b0.05}^{3/4}}{(1+z)^{3/8}} \left( \frac{\ln(1+C_0)}{\ln(1+C)} \right)^{3/4}, \quad (\text{B17})$$

where  $Z_{0.2} \equiv Z/(0.2Z_{\odot})$  and  $f_{b0.05} \equiv f_b/0.05$ . In this formula, following Dekel & Birnboim (2006), the variation of mean metallicity with redshift can be crudely approximated by

$$\log \frac{Z}{Z_0} = -0.17 z. \quad (\text{B18})$$

Following Bullock et al. (2001), the average halo concentration near  $M \sim 10^{12} M_{\odot}$  is evolving as

$$C = C_0 (1+z)^{-1}, \quad C_0 \simeq 13. \quad (\text{B19})$$

With this choice, the critical mass is  $M_{\text{sh}} \sim 10^{12} M_{\odot}$  and is only a weak function of redshift. It becomes even weaker if  $f_b$  gets slightly higher at high  $z$ . One can see that a factor of 4 change in the unknown  $Z_0$  results in a factor of  $\sim 2$  in  $M_{\text{sh}}$ .

Another uncertainty, which is explicit in the FHM recipe, is in the actual SFR that is associated with the maximum possible rate provided by the disc accretion rate. This can be modeled as a free ratio, smaller than unity, between the two.